Islamic University Journal of Applied Sciences (IUJAS)
https://journals.iu.edu.sa/jesc

Volume VII, Issue I, 1 July 2025, Pages 168-180

Photovoltaic Cells Fed a Dual Open-End Winding Induction Motor Driven by Fuzzy Field-Oriented Control

Mourad Sellah [1, *], Ahmed Lamine Dourari [2], Hakim Bagua [3]

[1] Faculty of Science and Technology, University of Ghardaïa, Algeria, mourad.sellah@yahoo.fr
[2] Faculty of Science and Technology, University of Sidi Bel Abbes, Algeria, lamine.dourari@gmail.com
[3] Faculty of Science and Technology, University of Ouargla, Algeria, hakim90mahi@gmail.com

*Corresponding author: (M. Sellah), *Email Address*: mourad.sellah@yahoo.fr

Abstract

The study presented in this article focuses on photovoltaic solar panels (PV) powering a Dual Open-End Winding Induction Motor (DOEWIM) fed by four three-phase inverters. Field Oriented Control (FOC) is adopted to regulate the stator current, rotor flux and rotation speed of the proposed machine, and Maximum Power Point Tracking (MPPT) technique is used to maximize power output from the solar panel. In order to achieve high performances in terms of fast dynamic speed response and best disturbance rejection, Fuzzy Logic Controller (FLC) is used for speed regulation. The main objective of this work is to introduce renewable energies into the drive of induction motors, especially those with open windings, in order to obtain several advantages, such as obtaining more robust performance towards external and internal disturbances, reduction of torque and flux ripples, minimization of stator current harmonics, and elimination of common mode voltage (CMV). The results obtained demonstrated the realization of the main advantages mentioned above, which confirms the validity of the proposed control on the topology of the induction motor studied.

Keywords: Photovoltaic, Maximum power point tracking, Field oriented control, Open-end winding, Fuzzy logic controller

https://doi.org/10.63070/jesc.2025.011
Received 25 April 2025; Revised 21 May 2025; Accepted 25 May 2025.
Available online 28 May 2025.

1. Introduction

Over the past century, global energy consumption has grown irrationally and continues to rise across all regions. As energy demand is expected to keep increasing, it is crucial to reassess our resource use to achieve truly sustainable and environmentally friendly development [1]. The depletion of fossil fuels and the associated greenhouse gas emissions highlight the urgent need to develop alternative energy sources. Among these, renewable energy stands out as a viable, eco-friendly substitute for fossil and nuclear energy, offering advantages such as being natural, inexhaustible, and well-suited for decentralized generation. Photovoltaic (PV) energy is one of the most promising forms of renewable energy, converting sunlight into electricity using solar panels composed of interconnected solar cells. PV systems have minimal environmental impact—they operate silently, discreetly, and without visual pollution [2]. A key feature of most PV systems is the implementation of a technique known as Maximum Power Point Tracking (MPPT), which continuously adjusts system parameters to ensure the panel operates at its maximum power output.

In recent years, multi-phase machines have gained significant attention from researchers, manufacturers, and industry professionals due to their ability to overcome several limitations associated with conventional three-phase machines. By increasing the number of phases, these machines distribute power and current more evenly, reducing stress on switches and windings. This design also leads to lower torque ripple, improved torque smoothness, and enhanced reliability enabling continued operation even when one or two non-adjacent phases fail [3, 4]. These benefits make multi-phase machines robust, low-maintenance, and scalable, supporting their growing use in high-power applications such as railway traction, naval propulsion, compressors, and cement mills [4, 5]. A prominent example is the Dual Star Induction Machine (DSIM), a six-phase machine consisting of two offset three-phase stator windings in the fixed part. This configuration combines the advantages of traditional induction machines with the added benefits of multi-phase operation [6]. To further enhance its performance and reliability, the DSIM can be modified into a Dual Open-End Winding Induction Machine (DOEWIM) by separating the connections of both stator windings [7]. This topology requires control via four three-phase voltage sources with carefully calculated phase shifts to eliminate common-mode voltage—thereby mitigating issues like bearing currents and shaft voltages, which are major contributors to premature machine failures [8-9].

Advancements in power electronics and modern control strategies have enabled AC drives to achieve dynamic performance levels comparable to those of DC drives—without the drawbacks associated with brushes and commutators. The main challenge in controlling asynchronous (AC) machines lies in the complex coupling between torque and magnetic flux. Field-Oriented Control (FOC) addresses

this by decoupling torque and flux control, effectively emulating the behavior of a separately excited DC motor. With FOC and the integration of powerful microprocessors, precise control of speed and torque in AC machines is now possible, matching the performance traditionally associated with DC machines [10].

To achieve high performance and robustness under varying operating conditions, advanced control methods like fuzzy logic controllers (FLC) have been proposed as alternatives to traditional PI controllers. FLCs offer several advantages over PI and PID controllers [11]. They allow the integration of human expertise through linguistic rules and can implement nonlinear control strategies without requiring an exact mathematical model of the system. Additionally, FLCs exhibit strong robustness, though their response may vary significantly with changes in system parameters.

This article is organized into five main sections. The first introduces the photovoltaic system and the MPPT technique used to optimize panel output. The second section describes the DOEWIM, highlighting its dual stator winding configuration. The third section outlines the indirect field-oriented control strategy and its key features. In the fourth section, the conventional IFOC is enhanced by replacing the traditional speed controller with a fuzzy logic-based regulator to improve system robustness. The fifth section presents simulation results, offering a detailed performance analysis under various practical scenarios. The article concludes with future perspectives and potential directions for further research.

2. Photovoltaic system and MPPT technique

2.1 Equivalent diagram of a solar cell

A single-diode equivalent circuit is the most commonly used model for representing a solar cell. In this model, the short-circuit current generated by illumination is represented as a current source, while the photovoltaic effect is modeled by a diode. Additionally, a series resistance and a parallel (shunt) resistance are included to account for the losses in the system. Figure 1 shows the equivalent circuit of the photovoltaic cell model [12,13].

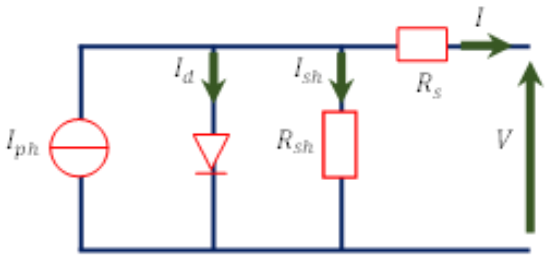

Figure 1. Equivalent PV cell circuit.

The characteristic equations of a solar cell are given by:

$$\begin{cases} I = I_{ph} - I_d - I_{sh} \\ I_d = I_0\left(e^{\left[\frac{q(V+R_sI)}{kAT}-1\right]}\right) \\ I_{sh} = \frac{V+R_sI}{R_{sh}} \end{cases} \quad (1)$$

2.2 Perturb and Observe algorithm (P&O)

Due to its simplicity and ease of implementation, the Perturb and Observe (P&O) method is one of the most widely used MPPT techniques. Its principle is based on introducing a small disturbance in the DC voltage of the PV array and observing the resulting variation in the output power.

If the power increases following the disturbance, the system continues perturbing in the same direction. Otherwise, the direction of the disturbance is reversed. When a power increase is observed, the operating point lies to the left of the maximum power point (MPP). Conversely, if the disturbance causes a decrease in power, it indicates that the MPP has been crossed and the operating point is now on the right side of the MPP [14].

In such cases, the algorithm reverses the perturbation direction to track the MPP more effectively. Once the MPP is reached, the operating point stabilizes at the maximum power output.

3. Description and modelling of DOEWIM

The DOEWIM is a DSIM with open stator windings and, therefore, consists of twelve stator terminals six for each winding forming two identical star configurations that share the same stator and are electrically shifted by an angle of $\pi/6$ radians.

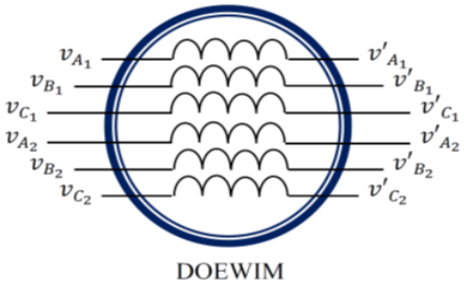

Figure 2. Voltage supply dual open-end winding induction motor.

Hence, four groups of three terminals are obtained, which require four three-phase converters to ensure powering and controlling the studied machine.

Consider $v_{a1}, v_{b1}, v_{c1}, v'_{a1}, v'_{b1}$ and v'_{c1} are respectively the pole voltages at the six outputs of the first two converters that are feeding the first ends of the two-stator winding, and $v_{a2}, v_{b2}, v_{c2}, v'_{a2}, v'_{b2}$ and v'_{c2} are respectively the pole voltages at the six outputs of the second two converters that are feeding the second ends of the two previous stator winding, as shown in the Figure 2.

The voltage across each phase winding among the six phases of the studied motor can be obtained based on the difference between the corresponding terminal voltages applied to its ends, as follows:

First stator: $\begin{cases} V_{A_1} = v_{A_1} - v'_{A_1} \\ V_{B_1} = v_{B_1} - v'_{B_1} \\ V_{C_1} = v_{C_1} - v'_{C_1} \end{cases}$ (2)

Second stator: $\begin{cases} V_{A_2} = v_{A_2} - v'_{A_2} \\ V_{B_1} = v_{B_2} - v'_{B_2} \\ V_{C_1} = v_{C_2} - v'_{C_2} \end{cases}$ (3)

Based on these assumptions, the DOEWIM model in the (d, q) frame can be presented as follows:

The stator and rotor voltages equations

$$\begin{cases} V_{ds_1} = R_{s_1}\iota_{ds_1} + \dot{\varphi}_{ds_1} - \omega_s\varphi_{qs_1} \\ V_{qs_1} = R_{s_1}\iota_{qs_1} + \dot{\varphi}_{qs_1} + \omega_s\varphi_{ds_1} \\ V_{ds_2} = R_{s_2}\iota_{ds_2} + \dot{\varphi}_{ds_2} - \omega_s\varphi_{qs_2} \\ V_{qs_2} = R_{s_2}\iota_{qs_2} + \dot{\varphi}_{qs_2} + \omega_s\varphi_{ds_2} \\ V_{dr} = R_r\iota_{dr} + \dot{\varphi}_{dr} - (\omega_s - \omega_r)\varphi_{qr} = 0 \\ V_{qr} = R_r\iota_{qr} + \dot{\varphi}_{qr} + (\omega_s - \omega_r)\varphi_{dr} = 0 \end{cases} \quad (4)$$

With: $\begin{cases} V_{ds_1} = v_{ds_1} - v'_{ds_1} \\ V_{qs_1} = v_{qs_1} - v'_{qs_1} \\ V_{ds_2} = v_{ds_2} - v'_{ds_2} \\ V_{qs_2} = v_{qs_2} - v'_{qs_2} \end{cases}$

The stator and rotor flux equations

$$\begin{cases} \varphi_{ds_1} = L_{s_1}\iota_{ds_1} + L_m(\iota_{ds_1} + \iota_{ds_2} + \iota_{dr}) \\ \varphi_{qs_1} = L_{s_1}\iota_{qs_1} + L_m(\iota_{qs_1} + \iota_{qs_2} + \iota_{qr}) \\ \varphi_{ds_2} = L_{s_1}\iota_{ds_2} + L_m(\iota_{ds_1} + \iota_{ds_2} + \iota_{dr}) \\ \varphi_{qs_2} = L_{s_2}\iota_{qs_2} + L_m(\iota_{qs_1} + \iota_{qs_2} + \iota_{qr}) \\ \varphi_{dr} = L_r\iota_{dr} + L_m(\iota_{ds_1} + \iota_{ds_2} + \iota_{dr}) \\ \varphi_{qr} = L_r\iota_{qr} + L_m(\iota_{qs_1} + \iota_{qs_2} + \iota_{qr}) \end{cases} \quad (5)$$

The mechanical equation

$$\frac{J}{P}\frac{d\omega_r}{dt} = T_{em} - T_L - \frac{K_f}{P}\omega_r \quad (6)$$

4. Field oriented control

Indirect Field-Oriented Control (IFOC) eliminates the need for flux sensors by using known motor parameters to calculate the appropriate slip frequency, thereby determining the desired flux position [15,16]. In this method, rotor flux is estimated based on the stator current vector, voltage vector, and rotor speed, and this estimation is then provided to the flux and torque controllers [17]. This approach is simpler to implement than the direct FOC method and can operate effectively across the full speed range from zero to high speed in both directions. As a result, the indirect vector control method is gaining increasing popularity.

The equations system for stator voltages is given by:

$$\begin{cases} v_{ds_1} = R_{s_1}\iota_{ds_1} + L_{s_1}i_{ds_1} - \omega_s^*\left(L_{s_1}\iota_{qs_1} + \tau_r\varphi_r^*\omega_{gl}^*\right) \\ v_{qs_1} = R_{s_1}\iota_{qs_1} + L_{s_1}i_{qs_1} - \omega_s^*\left(L_{s_1}\iota_{ds_1} + \varphi_r^*\right) \\ v_{ds_2} = R_{s_2}\iota_{ds_2} + L_{s_2}i_{ds_2} - \omega_s^*\left(L_{s_2}\iota_{qs_2} + \tau_r\varphi_r^*\omega_{gl}^*\right) \\ v_{qs_2} = R_{s_2}\iota_{qs_2} + L_{s_2}i_{qs_2} - \omega_s^*\left(L_{s_2}\iota_{ds_2} + \varphi_r^*\right) \end{cases} \quad (7)$$

The electromagnetic torque expression is as follows:

$$T_{em}^* = P\frac{L_m}{L_m+L_r}\left[\left(\iota_{qs_1} + \iota_{qs_2}\right)\varphi_r^*\right] \quad (8)$$

The rotor flux is regulated by a defluxing block, where, in general, the flux is maintained at its nominal value during operation at or below the machine's nominal speed. In cases where the operating speed exceeds the nominal speed, the flux is reduced to limit the machine's voltage. The reference flux is defined as follows:

$$\begin{cases} \varphi_r^* = \varphi_n \quad si \quad |\Omega| \le \Omega_n \\ \varphi_r^* = \frac{\varphi_n\Omega_n}{|\Omega|} \quad si \quad |\Omega| > \Omega_n \end{cases} \quad (9)$$

Defluxing allows optimal exploitation of the machine's magnetic capabilities at under speed ($|\Omega| \le \Omega_n$) and overspeed ($|\Omega| > \Omega_n$).

5. Fuzzy logic controller

5.1 Fuzzy logic controller and its main steps

The fuzzy logic controller uses a set of fuzzy rules that represent a decision-making mechanism to adjust the system's response to various stimuli. The primary goal of using an FLC is to replace a skilled human operator with a rule-based fuzzy system. Fuzzy logic provides a convenient method for mapping input variables to output responses [18–23] and is conceptually straightforward to understand [24–28].

A typical fuzzy logic controller consists of three main steps:

Fuzzification

The most common controller has two inputs, error and the derivative of the error with respect to a defined reference signal and one output, which is usually the control command.

Fuzzy inference engine

The fuzzy rule consists of an antecedent–consequent pair, expressed as IF-THEN rules encoded in a lookup table (Table 1). The input-output mapping is performed using an inference mechanism based on Zadeh's logic.

Table 1. Inference rules table.

ce \ e	NB	NM	NS	ZE	PS	PM	PB
NB	NB	NB	NB	NB	NM	NVS	ZE
NM	NB	NB	NB	NM	NVS	ZE	PVS
NS	NB	NB	NM	NVS	ZE	PVS	PM
ZE	NB	NM	NVS	ZE	PVS	PM	PB
PS	NM	NVS	ZE	PVS	PM	PB	PB
PM	NVS	ZE	PVS	PM	PB	PB	PB
PB	ZE	PVS	PM	PB	PB	PB	PB

Fuzzy inference engine

The center of area defuzzification method is used to calculate the crisp output value.

5.2 Computational cost of the fuzzy logic controller

The computational cost of a fuzzy logic controller can be relatively high, especially in real-time control scenarios, due to the complexity of fuzzification, inference, and defuzzification operations. Unlike conventional controllers such as PI, a fuzzy controller requires the evaluation of multiple linguistic rules and the execution of nonlinear calculations at each sampling cycle. This computational load can be a challenge for embedded systems or applications requiring very fast response times. However, with advancements in microcontrollers and digital signal processors (DSPs), it is now possible to efficiently implement fuzzy controllers in real-time systems, provided the algorithms are optimized and the number of rules is kept within reasonable limits.

Figure 3 shows the general diagram of the control structure using the fuzzy field-oriented control technique for a DOEWIM supplied by two photovoltaic solar panels, with speed, rotor flux, and stator currents controlled in a nonlinear control plane.

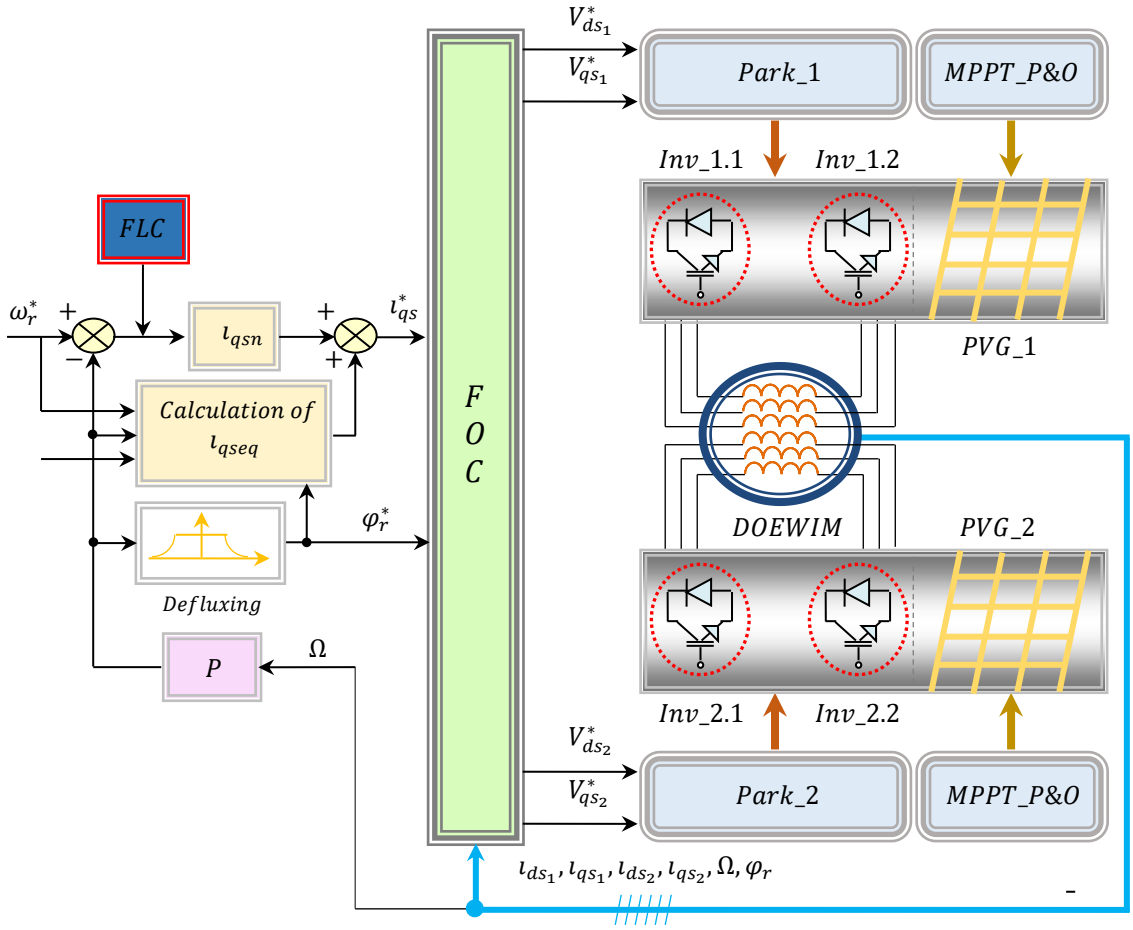

Figure 3. Fuzzy field-oriented control scheme applied on DOEWIM powered by photovoltaic cells.

6. Simulation results and discussions

In this section, the application of fuzzy field-oriented control for the operation of the DOEWIM powered by photovoltaic cells is examined through simulation tests.

The main objective is to present a detailed analysis of the performance of this control technique by studying the dynamic behavior of key electrical, electromagnetic, and mechanical variables, such as stator current, electromagnetic torque, stator flux, and rotor speed. Additionally, tests were conducted for different reference speed values, considering start-up under no load, load torque application, and speed reversal.

Indeed, these simulations include a sequence of steps that can imitate the practical cases in industrial applications. The machine starts up at $t = 0s$ with no load following an imposed reference speed profile of $150rad/s$, at $t = 1s$ a load torque of $T_L = 5N.m$ is applied which is considered as an external perturbation, at $t = 1.5s$ the reference speed value is increased to $200rad/s$ then at $t = 2s$

the applied load torque is increased to $T_L = 10\ Nm$, then at $t = 3s$ the applied load torque is removed which means that $T_L = 0N.m$.

The second part of these simulations present the dynamic behaviour of the proposed control technique against the speed revers, where at $t = 3s$ the reference speed is inverted to a value of $-150rad/s$ without the application of any load torque, then at $t = 5s$ another value of the inverted reference speed is applied to become $-200\ rad/s$.

Figure 4 shows the rotor speed and its reference for the fuzzy field-oriented control applied to the DOEWIM. Note that the four passages from $0rad/s$ to $150rad/s$ then from $150rad/s$ to $200rad/s$ on the one hand, and from $200rad/s$ to $-150rad/s$, then from $-150rad/s$ to $-200rad/s$ on the other hand are carried out by the rotor speed in a linear manner without any overshoot, completely identical to the practical case. In the steady state, the rotor speed perfectly follows the reference speed without showing a real influence for different load applications, moreover the error representing the difference between the two speeds is very low. Overall, the rotor speed response is very satisfactory at all stages of operation, indicating the robustness and accuracy of the fuzzy logic controller.

Figure 5 gives the electromagnetic torque developed by the machine studied. The electromagnetic torque exhibits high dynamics characterized by minimal fluctuations. The width of the torque fluctuation band appears very small, which confirms the precision of the proposed control by eliminating fluctuations. The torque response to the application of loads and to the reversal of direction of rotation is carried out with great precision and without any overshoot thanks to the great robustness of the field-oriented control.

The stator phase currents of the first DOEWIM star are shown in Figure 6. At start-up, the currents are unequal due to the induction of the circuit, then in the equilibrium state the amplitude of these currents is constant, then, when the load is introduced or the direction of rotation is reversed, the amplitudes currents increase, which suggests a strong performance of the field-oriented control.

The components of the direct and quadratic rotor flux for the DOEWIM powered by photovoltaic cells are represented by Figure 7. We note that the two components φ_{dr} and φ_{qr} pass a very short-term transient regime then reach perfect stability successively at the values $1Wb$ and $0Wb$ in steady state, which proves that the complete decoupling between the torque and the flux is maintained by field-oriented command.

Figure 8 clearly shows the chosen irradiation (E) values, which varied between $600W/m^2$ and $800W/m^2$. Observation of Figure 9 and Figure 10, which represent the voltage and the power of photovoltaic generator respectively, confirms that the irradiation value is directly proportional to the

voltage and the power of photovoltaic generator, since as the irradiation increases, the voltage and the power of photovoltaic generator increase, and vice versa.

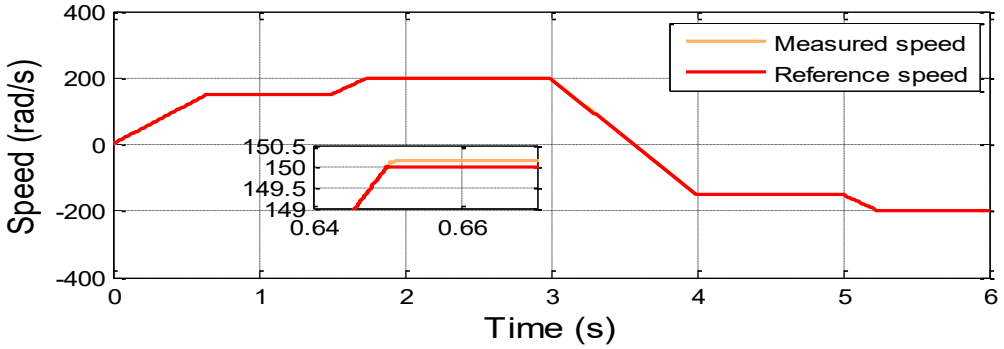

Figure 4. Rotor speed of the DOEWIM.

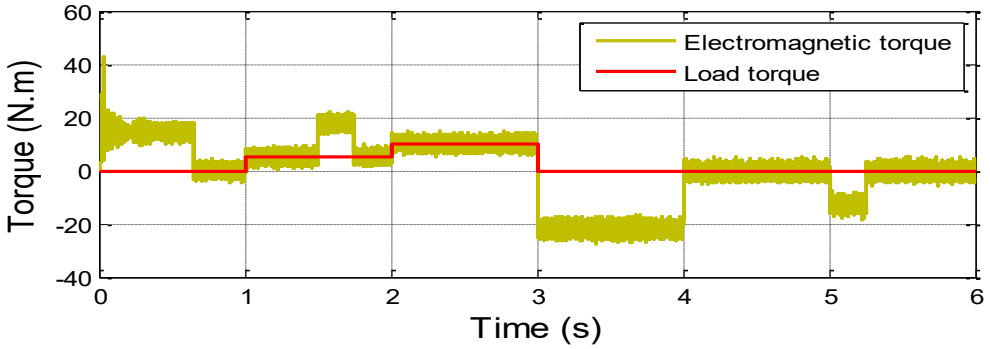

Figure 5. Electromagnetic torque developed by the DOEWIM.

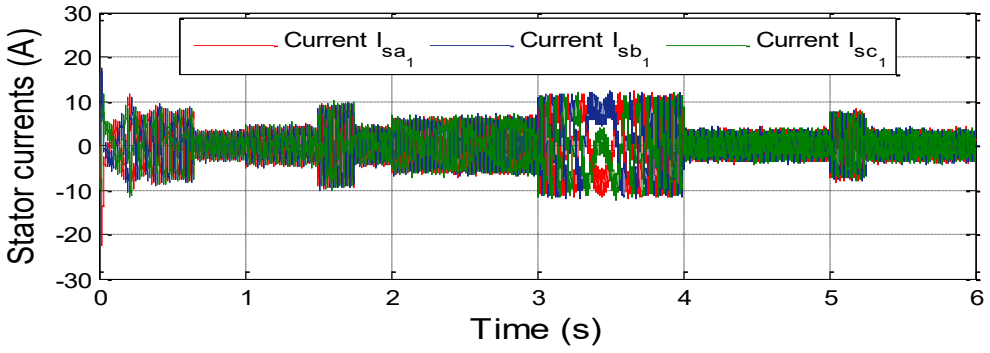

Figure 6. Stator phase currents.

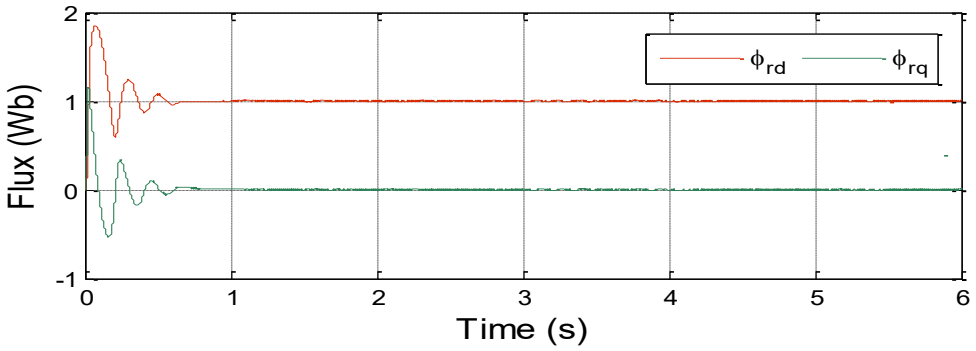

Figure 7. Components of the rotor flux.

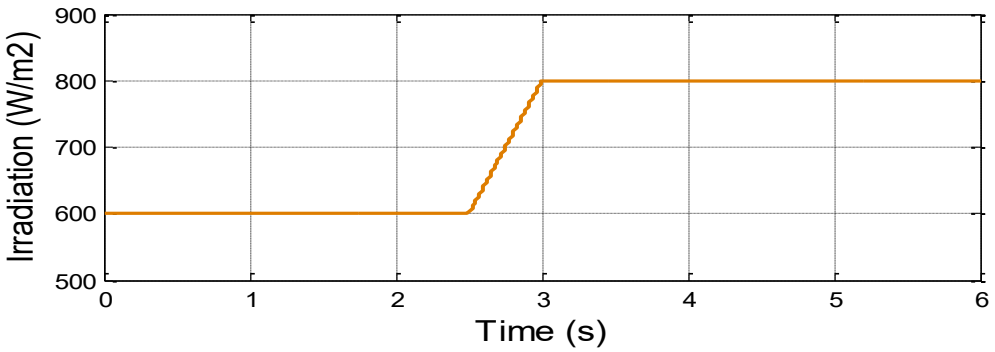

Figure 8. Solar irradiation.

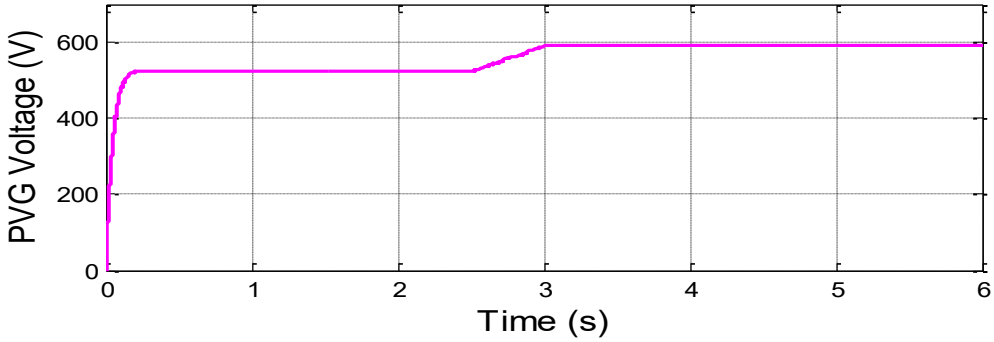

Figure 9. PVG Voltage.

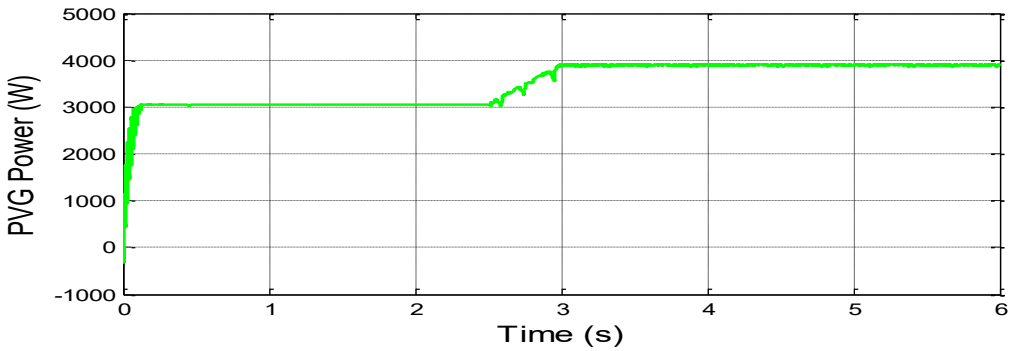

Figure 10. PVG Power.

7. Conclusion

In conclusion, the proposed control technique proves to be a highly competitive and promising solution for the control of multiphase machines, particularly those with open stator winding topologies. Notably, the application of this control strategy to the DOEWIM powered by photovoltaic energy represents a novel contribution, as such integration has not been thoroughly explored in existing literature. The simulation results obtained using the artificial intelligence-based control method developed in this study highlight significant improvements in system performance, demonstrating both enhanced dynamic response and high operational efficiency under various demanding conditions.

This control approach effectively addresses many of the key challenges typically encountered in multiphase machine control such as complexity, nonlinearity, and fault tolerance making it especially suitable for high-power industrial applications where system reliability, minimal maintenance, and uninterrupted operation are critical. Therefore, the proposed technique holds strong potential for future deployment in real-world scenarios requiring robust, intelligent, and energy-efficient control systems.

References

[1] Onyinyechukwu C., Cosmas Dominic D., and All. ‘‘Control systems in renewable energy: A review of applications in Canada, USA, and Africa ‘‘. World Journal of Advanced Engineering Technology and Sciences, 2024, 11(01), 029–036.
[2] Malhar K., Muhammad Amir R., Muhammad F., and All.” Conventional and artificial intelligence based maximum power point tracking techniques for efficient solar power generation ‘‘, Engineering Reports, Wiley. June 2024.
[3] Kali, Y.; Saad, M.; Doval-Gandoy, J.; Rodas, J. Discrete Terminal Super-Twisting Current Control of a Six-Phase Induction Motor. Energies 2021, 14, 1339.
[4] Kali, Y.; Ayala, M.; Rodas, J.; Saad, M.; Doval-Gandoy, J.; Gregor, R.; Benjelloun, K. Current Control of a Six-Phase Induction Machine Drive Based on Discrete-Time Sliding Mode with Time Delay Estimation. Energies 2019, 12, 170.
[5] Marouani, K.; Baghli, L.; Hadiouche, D.; Kheloui, A.; Rezzoug, A. A New PWM Strategy Based on a 24-Sector Vector Space Decomposition for a Six-Phase VSI-Fed Dual Stator Induction Motor. IEEE Trans. Ind. Electron. 2008, 55, 1910–1920.
[6] Rahali, H.; Zeghlache, S.; Benyettou, L.; Benalia, L. Backstepping Sliding Mode Controller Improved with Interval Type-2 Fuzzy Logic Applied to the Dual Star Induction Motor. Int. J. Comput. Intell. Appl. 2019, 18, 1950012.
[7] Nirsha, K.I.; Rajeevan, P.P. A direct torque control scheme for dual inverter fed induction motor drive with a common DC voltage source. In Proceedings of the IECON 2017—43rd Annual Conference of the IEEE Industrial Electronics Society, Beijing, China, 29 October–1 November 2017.
[8] Ranjit, M.; Gowtami, S.; Babu, B.G. Reduction of zero sequence voltage using multilevel inverter fed open-end winding induction motor drive. Acta Electrotech. Inform. 2016, 16, 52–60.
[9] Foti, S.; Testa, A.; De Caro, S.; Scimone, T.; Scelba, G.; Scarcella, G. Multi-level open end windings multi-motor drives. Energies 2019, 12, 861.
[10] Ansari, S.; Chandel, A. Simulation based comprehensive analysis of direct and indirect matrix converter fed asynchronous motor drive. In Proceedings of the 2017 4th IEEE Uttar Pradesh Section International Conference on Electrical, Computer and Electronics (UPCON), Mathura, India, 26–28 October 2017.
[11] Benachour, A.; Berkouk, E.M.; Mahmoudi, M.O. Study and comparison between two DTC strategies of induction machine fed by direct matrix converter. J. Renew. Sustain. Energy 2017, 9, 55501.
[12] Van Huynh, V.; Nguyen, T.D.; Dao, V.-T.; Tran, Q.-H. An Efficient Carrier-Based Modulation Strategy for Five-Leg Indirect Matrix Converters to Drive Open-End Loads with Zero Common-Mode Voltage. Electr. Power Compon. Syst. 2019, 47, 1303–1315.
[13] Lavanya, N.; Rao, M.V.G. Control of indirect matrix converter by using improved SVM method. Int. J. Power Electron. Drive Syst. 2015, 6, 370–375.
[14] A. Levant, “Higher-order sliding modes, differentiation and output-feedback control”, International Journal of Control, vol. 76, no. 09-10, pp. 924-941, 2003.
[15] Laszlo Gyugyi, ‘’Static Power Frequency Changers: Theory, Performance and Applications’’, Book, New York: Wiley, c76, 1976.

[16] Marco Matteini, “Control Techniques for Matrix Converter Adjustable Speed Drives”, PhD thesis, Department of Electrical Engineering, University of Bologna, 2001.
[17] François Gruson, “Modulation Naturelle Généralisée des Convertisseurs Matriciels pour la Variation de Vitesse”, Thèse de doctorat, Ecole centrale de Lille, 2010.
[18] Arie Levant, “Higher Order Sliding Modes and Their Application for Controlling Uncertain Processes”, PhD theses, Institute for System Studies of the USSR Academy of Science, Moscow, 1987.
[19] Chennana, A., Megherbi, A. C., Bessous, N., Sbaa, S., Teta, A., Belabbaci, E. O., ... & Agajie, T. F. (2025). Vibration signal analysis for rolling bearings faults diagnosis based on deep-shallow features fusion. *Scientific Reports*, *15*(1), 9270.
[20] Bentegri, H., Rabehi, M., Kherfane, S., Nahool, T. A., Rabehi, A., Guermoui, M., ... & El-Kenawy, E. S. M. (2025). Assessment of compressive strength of eco-concrete reinforced using machine learning tools. *Scientific Reports*, *15*(1), 5017.
[21] Mehallou, A., M’hamdi, B., Amari, A., Teguar, M., Rabehi, A., Guermoui, M., ... & Khafaga, D. S. (2025). Optimal multiobjective design of an autonomous hybrid renewable energy system in the Adrar Region, Algeria. *Scientific Reports*, *15*(1), 4173.
[22] eddine Boukredine, S., Mehallel, E., Boualleg, A., Baitiche, O., Rabehi, A., Guermoui, M., ... & Tibermacine, I. E. (2025). Enhanced Performance of Microstrip Antenna Arrays through Concave Modifications and Cut-Corner Techniques. *ITEGAM-JETIA*, *11*(51), 65-71.
[23] Belaid, A., Guermoui, M., Riche, A., Arrif, T., Maamar, H., Kamel, C. M., ... & Al Rahhal, M. M. (2024). High-Resolution Mapping of Concentrated Solar Power Site Suitability in Ghardaïa, Algeria: A GIS-Based Fuzzy Logic and Multi-Criteria Decision Analysis. *IEEE Access*.
[24] Tibermacine, A., Akrour, D., Khamar, R., Tibermacine, I. E., & Rabehi, A. (2024, December). Comparative Analysis of SVM and CNN Classifiers for EEG Signal Classification in Response to Different Auditory Stimuli. In *2024 International Conference on Telecommunications and Intelligent Systems (ICTIS)* (pp. 1-8). IEEE.
[25] Mostefaoui, M., Belfedhal, A. E., Larbi, A. A., Rabehi, A., Abderrezzaq, Z., & Dabou, R. (2024, December). Enhanced Detection of EVA Discoloration Defects in Solar Cells Using Vision Transformers and Contrastive Learning. In *2024 International Conference on Telecommunications and Intelligent Systems (ICTIS)* (pp. 1-6). IEEE.
[26] Tibermacine, A., Tibermacine, I. E., Zouai, M., & Rabehi, A. (2024, December). EEG Classification Using Contrastive Learning and Riemannian Tangent Space Representations. In *2024 International Conference on Telecommunications and Intelligent Systems (ICTIS)* (pp. 1-7). IEEE.
[27] Ladjal, B., Tibermacine, I. E., Bechouat, M., Sedraoui, M., Napoli, C., Rabehi, A., & Lalmi, D. (2024). Hybrid models for direct normal irradiance forecasting: A case study of Ghardaia zone (Algeria). *Natural Hazards*, *120*(15), 14703-14725.
[28] Belaid, A., Guermoui, M., Khelifi, R., Arrif, T., Chekifi, T., Rabehi, A., ... & Alhussan, A. A. (2024). Assessing Suitable Areas for PV Power Installation in Remote Agricultural Regions. *Energies*, *17*(22), 5792.